JOURNAL OF GUIDANCE, CONTROL, AND DYNAMICS
Vol. 16, No. 3, May–June 1993

# Two-Axis Dry Tuned-Rotor Gyroscopes: Design and Technology

William M. Mansour
*McMaster University, Hamilton L8S 4L7, Ontario, Canada*
and
Corrado Lacchini
*DIGICON S.A., Gravatai 94000, Rio Grande de Sul, Brazil*

## Nomenclature

$a_X, a_Y, a_Z$ = linear accelerations applied to gyro case (m/s$^2$)
$B_a$ = magnetic field in radial gap (Weber/m$^2$)
$B_X, B_Y$ = bias associated with the $X$ and $Y$ axes (deg/h)
$cx_i, cy_i$ = constant coefficient in power series expansion; Eq. (15), $i = 0, 1, 2, \ldots$.
$D_R$ = damping coefficient for rotor to case about $X_R, Y_R$ (N·m·s/deg)
$D_X, D_Y$ = damping coefficient for flexures about $X_G, Y_G$ (N·m·s/deg)
$d$ = offset distance (m) as in Fig. 10
$d_b$ = diameter of bare wire of torquer coil (m)
$d_c$ = distance between two opposite coils (m) as shown in Fig. 8
$d_X, d_Y$ = ($1\sigma$) values of repeatability (deg/h)
$E$ = voltage across torquer coil (V)
$e$ = offset distance (m) as in Fig. 10
$F$ = force of interaction of magnetic field and current $i_t$ in the torquer coil (N)
$g$ = local gravitational acceleration (m/s$^2$)
$g_{X1}, g_{X2}$ = gaps associated with opposite pickoffs (m)
$H$ = magnitude of angular-momentum vector $\boldsymbol{H}$ of the rotor (kg·m$^2$/s) = $J_Z \cdot \omega_S$
$h$ = coefficient of convective heat transfer for torquer coil (cal/s·m$^2$·°C)
$i_t$ = current in torquer coil (A)
$I_X, I_Y, I_Z$ = moments of inertia of the gimbal about $X_R, Y_R, Z_R$ (kg·m$^2$)
$J_X, J_Y, J_Z$ = moments of inertia of rotor about $X_R, Y_R, Z_R$ (kg·m$^2$)
$K_1, K_2, K_3$ = rotor's suspension stiffness about axes 1,2,3 (N/m)
$k_1, k_2, k_3$ = gimbal's suspension stiffness about axes 1,2,3 (N/m)
$K_X, K_Y$ = torsional stiffness of flexures about $X_G, Y_G$ (N·m/deg)
$\ell_c$ = curved length of coil (m)
$m$ = direct drift (deg/h)
$mm$ = number of off-on cycles for day-to-day drift tests
$n$ = number of turns in torquer coil
$nn$ = number of data points for a random drift test
$P_m$ = mean perimeter of torquer coil (m)
$q$ = quadrature drift (deg/h)
$R$ = torquer coil resistance ($\Omega$)
$R_X, R_Y$ = $X$ and $Y$ torquer resistances ($\Omega$)
$r_X, r_Y$ = ($1\sigma$) values of random drifts (deg/h)
$S_X, S_Y$ = $X$ and $Y$ torquer scale factors (deg/h·A)
$t$ = time (s)
$T_D$ = rotor-to-case drag torque (N·m)
$T_X, T_Y$ = moments applied to the rotor about $X, Y$ by the torquers (N·m)
$W_r$ = weight of rotor (N)
$X_j, Y_j$ = $X$ and $Y$ torquer currents in gyro testing (A); $j = 1,2,\ldots$
$X_C, Y_C, Z_C$ = coordinate set fixed to the gyro case; $Z_C$ along shaft
$X_G, Y_G, Z_G$ = coordinate set fixed to the gimbal; $X_G, Y_G$ along inner and outer flexures
$X_R, Y_R, Z_R$ = coordinate set fixed to, but not rotating with, the rotor; $Z_R$ along the spin axis of the rotor
$\delta_{Xg}, \delta_{Yg}$ = $g$-sensitive drifts (deg/h/$g$)
$\delta_{Xgg}, \delta_{Ygg}$ = $g^2$-sensitive drifts (deg/h/$g^2$)
$\theta, \theta_s$ = average temperature of torquer coil (°C)

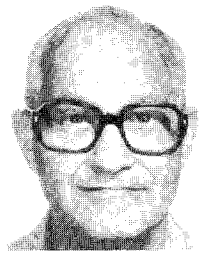

**William M. Mansour was born in Cairo, Egypt, on June 15, 1930. He received a B.Sc. in Mechanical Engineering in 1951 from Cairo University and a Ph.D. in 1963 from Toronto University, Canada. He has worked as a professor at Carleton, Concordia, Waterloo, and McMaster Universities in Canada and UFRJ and ITA in Brazil. He is the author of more than sixty papers and winner of the first prize for best paper on "Gyroscopic Tracking" in the ASME International Congress on Mechanisms in 1972. He worked as a Senior Researcher and as a technical consultant on the design of gas turbines for UNITED AIRCRAFT of Canada and on inertial navigation systems for Centro Tecnologico Aerospacial (CTA), AVIBRAS, and DIGICON in Brazil.**

**Corrado Lacchini was born in Reggio Emilia, Italy, in June 1943. He graduated in 1961 from Instituto Tecnico Industriale e Conti in Milan and then completed his specialization in 1964 in Industrial Automation at the Instituto A Beltrami, also in Milan. From 1961 to 1969 he worked as a designer for machine automation in Pirelli and as a designer for automatic test equipment for computers in Olivetti-electronics. He worked until 1977 for Olivetti-numerical control as a chief designer of a new family of controls. He joined DIGICON in 1977 to become the technical director responsible for the design and development of components for industrial automation and inertial navigation.**

Received Jan. 20, 1992; revision received April 12, 1992; accepted for publication April 21, 1992. 

$\dot{\theta}_X, \dot{\theta}_Y$ = angular velocities of the rotor relative to $X_C, Y_C$ (rad/s)
$\dot{\phi}_X, \dot{\phi}_Y, \dot{\phi}_Z$ = $\omega_x, \omega_Y, \omega_Z$ = angular velocities of the gyro case relative to $X_C, Y_C, Z_C$ (rad/s)
$\Lambda$ = Earth's rotation (deg/h)
$\lambda$ = latitude of supplier's laboratory (deg)
$\rho$ = weight of gimbal/weight of rotor
$\rho_e$ = specific resistance of wire of torquer coil ($\Omega \cdot$m)
$\tau_r$ = runup time (s)
$\psi$ = error angle (deg) as in Fig. 10
$\omega_D$ = dynamic range of DTG (deg/s)
$\omega_S$ = speed of the shaft rotation relative to the case (rad/s)

## Introduction

THE dry tuned-rotor gyro (DTG) is a two-degree-of-freedom sensor of angular velocities about two mutually orthogonal axes. It is a relatively recent development in conventional sensor technology. The first tuned two-axis oscillatory gyro was developed in 1945 by the Royal Aircraft Establishment (RAE) in England and was reported in a technical note[1] in 1948. The first oscillogyro was patented by Barnes.[2] Other variations of the DTG were patented by Howe,[3,4] Krupick et al.[5] and Erdley.[6]

This class of instrument has been adopted for the control of tracking radar systems; the perforation of petroleum wells; the navigation of ships, aircraft, helicopters, and terrestrial vehicles. Its major application is encountered in the guidance of unmanned space and underwater vehicles. Figure 1 shows the schematics of a DTG, which consist of

1) *Gyro case subassembly*, which houses a pair of ball bearings that, in turn, support the spin shaft. Also attached to the case is the stator of the hysteresis motor. Attached to the spin shaft is the stop and the hysteresis ring.

2) *Rotor hinge subassembly* containing the permanent magnets that are fixed to the rotor.

3) *Torquer pickoffs subassembly* that is attached to the gyro case. When an angular displacement is imparted to the gyro case shown in Fig. 1, about a line perpendicular to the plane of the paper, the axis of rotation of the rotor will remain fixed in inertial space due to the presence of an angular-momentum vector along that axis. The difference in the gaps will be sensed by the pickoffs. The signals from the pickoffs are used to inject a current in a pair of torquer coils that impart a correcting torque to the rotor. The latter is forced to precess in such a way as to minimize the difference of the gaps. The time integral of the current can be shown to be proportional to the angular deflection of the gyro case.

Figure 2 shows a typical functional block diagram for the gyro and the associated feedback loops. The output signal of

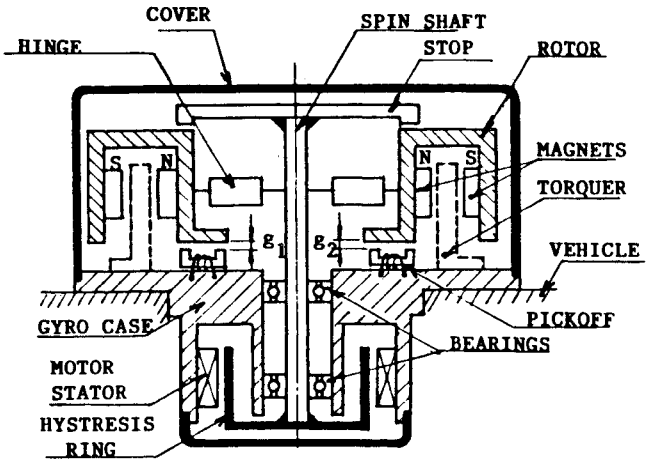


Fig. 1 Dry tuned-rotor gyro (DTG).

the $X$ pickoffs is demodulated, conditioned, amplified, and then fed back to the $Y$ torquer. A similar treatment is applied to the signal of the $Y$ pickoffs before feeding it back to the $X$ torquer. The output currents of the amplifiers are proportional to the angular velocity of the vehicle in two mutually perpendicular directions. The basic characteristics of a DTG are reported to the user in the following form: 1) *physical*: diameter, length, weight, type of connector; 2) *spin motor*: number of phases, excitation frequency, voltage; 3) *torquer and pickoffs*: scale factor, resistance, axis misalignment, continuous dynamic range; 4) *drifts*: non-$g$-, and $g$-sensitive (these are compensable); 5) *drifts*: day-to-day and random (these are noncompensable); and 6) *environmental*: temperature range, shock, random vibrations. The scale factor is the coefficient that relates the value of the current in the torquer coil to the angular velocity that is applied to the gyro case. The dynamic range is the maximum angular velocity that can be imparted to the gyro case and still be measured within a specified accuracy. The drifts are errors in the output signal of the gyro.

The DTG has several advantages. It requires no fluid to support. It is small in size, can resist radiation, and is amenable to thermal modeling. It can be used in a gimballed or strapdown system. It is low in cost per axis and of reliable technology. There are few suppliers in the world who dominate the technology of *inertial-quality* DTGs, i.e., DTGs of low drifts and high dynamic range. Brown[7] gave a list of such suppliers, together with the technical specifications for their products. DTGs that belong to this class are difficult to acquire and their price is high. This publication reports the latest advances in DTGs.

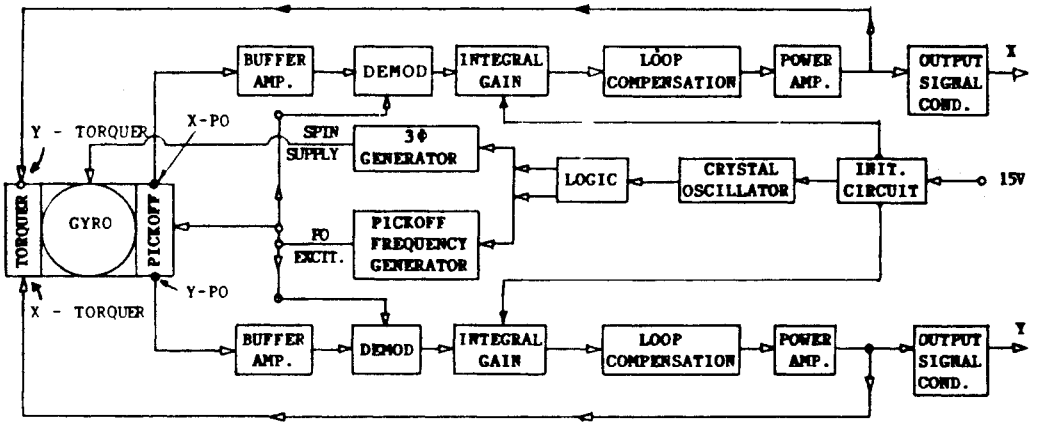


Fig. 2 Functional block diagram of a DTG.

## Equations of Motion

The complex dynamics of the DTG attracted the attention of several researchers in the past. Savet,[8] Lipman,[9] Craig,[10,11] Savage,[12] and Stieler and Winter[13] reported mathematical equations to describe the dynamics of the DTG. Other detailed studies were conducted and documented by NASA,[14] Teledyne,[15] Singer,[16] and an IEEE/ANSI Standard.[17] The equations reported were derived using the conventional approach and were neither simple to develop nor easy to use in their final forms.

Figure 3 shows the coordinate system used for the analysis of the flexure-mounted gyro. The mathematical model can be written in the following linearized form:

$$[M]\{\ddot{\theta}\} + [B]\{\dot{\theta}\} + [K]\{\theta\} = -[M]\{\ddot{\phi}\} - [N]\{\dot{\phi}\} - [L]\{\phi\} - \{T\} \quad (1)$$

Each of $M$, $B$, $K$, $N$, and $L$ is a $2\times 2$ matrix.

The elements of these matrices can be obtained by using any of the available computer routines that constructs the dynamic model of multibody systems starting from the definition of necessary coordinates, input stimuli, basic elements, and their interconnections. The authors of this paper used a routine developed by W. Schiehlen at the University of Stuttgart, Germany, to show that the elements of the previously mentioned matrices are given by

$$M_{11} = \alpha_1 + \alpha_2 \cdot C_2; \quad M_{12} = \alpha_2 \cdot S_2; \quad M_{21} = M_{12}$$

$$M_{22} = \alpha_1 - \alpha_2 \cdot C_2; \quad B_{11} = -2(\alpha_2 \cdot S_2)\omega_S + \gamma_1 \cdot C_2 + \gamma_2 + D_R$$

$$B_{12} = \alpha_3 + 2(\alpha_2 \cdot C_2)\omega_S + \gamma_1 \cdot S_2$$

$$B_{21} = -\alpha_3 - 2(\alpha_2 \cdot C_2)\omega_S + \gamma_1 \cdot S_2$$

$$B_{22} = 2(\alpha_2 \cdot S_2)\omega_S - \gamma_1 \cdot C_2 + \gamma_2 + D_R$$

$$K_{11} = -\alpha_4(1 + C_2)\omega_S^2 - \gamma_1 \cdot S_2 \cdot \omega_S + \beta_1 + \beta_2 \cdot C_2$$

$$K_{12} = -\alpha_4(S_2)\omega_S^2 + \gamma_1 \cdot C_2 \cdot \omega_S + \gamma_2 \cdot \omega_S + \beta_2 \cdot S_2 + T_D$$

$$K_{21} = -\alpha_4(S_2)\omega_S^2 - \gamma_1 \cdot C_2 \cdot \omega_S - \gamma_2 \cdot \omega_S + \beta_2 \cdot S_2 - T_D$$

$$K_{22} = -\alpha_4(1 - C_2)\omega_S^2 + \gamma_1 \cdot S_2 \cdot \omega_S + \beta_1 - \beta_2 \cdot C_2$$

$$N_{11} = -\alpha_5 \cdot S_2 \cdot \omega_S; \quad N_{12} = (\alpha_6 + \alpha_7 \cdot C_2)\omega_S$$

$$N_{21} = (-\alpha_8 + \alpha_7 \cdot C_2)\omega_S; \quad N_{22} = \alpha_7 \cdot S_2 \cdot \omega_S$$

$$L_{11} = 0; \quad L_{12} = 0; \quad L_{21} = 0; \quad L_{22} = 0 \quad (2)$$

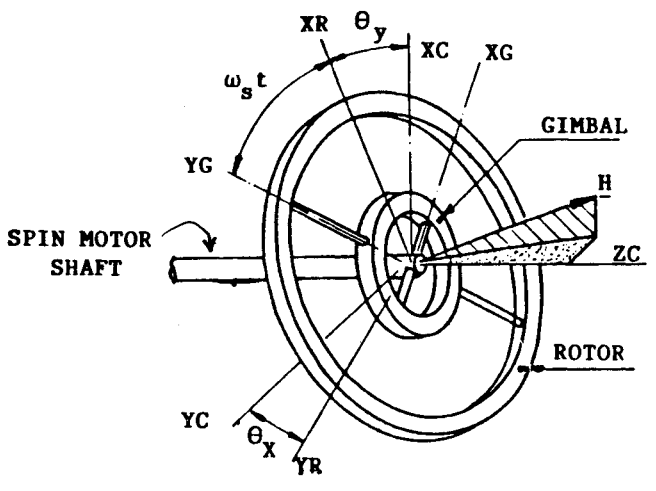


Fig. 3 Coordinate systems.

where

$$S_2 = \sin 2\omega_S \cdot t; \quad C_2 = \cos 2\omega_S \cdot t; \quad \alpha_1 = (I_X + J_X + J_Y)/2$$

$$\alpha_2 = (I_X + J_X - J_Y)/2; \quad \alpha_3 = (I_X + J_Z)\omega_S$$

$$\alpha_4 = (I_X + I_Y - I_Z)/2; \quad \alpha_5 = -J_X - J_Y + (I_X - I_Y + I_Z)/2$$

$$\alpha_6 = J_Z + (I_X - I_Y + I_Z)/2; \quad \alpha_7 = J_X - J_Y + (I_X - I_Y + I_Z)/2$$

$$\alpha_8 = J_Z + (I_X - I_Y - I_Z)/2; \quad \beta_1 = (K_X + K_Y)/2$$

$$\beta_2 = (K_X - K_Y)/2; \quad \gamma_1 = (D_X - D_Y)/2; \quad \gamma_2 = (D_X + D_Y)/2 \quad (3)$$

In using the computer routine, it was assumed that only the derivatives of $\{\phi\}$ are in existence as input stimuli. For this reason, the $L$ matrix was found to be identically zero. The model reported by relations (1–3) agrees with that derived by Craig.[10] Considering the gyro case to be moving on a steady course, i.e., the derivatives of $\{\phi\}$ are identically zero, and noting that

$$I_X = I_Y; \quad J_X = J_Y; \quad K_X = K_Y = K; \quad D_X = D_Y = D$$

the previous model can be arranged to read

$$(J_X + I_X/2)\ddot{\theta}_X + (D + D_R)\dot{\theta}_X + \{K - (I_X - I_Z/2)\omega_S^2\}\theta_X + (J_Z + I_X)\omega_S \cdot \dot{\theta}_Y + (T_D + D \cdot \omega_S)\theta_Y = q_X \cos 2\omega_S t - q_Y \cdot \sin 2\omega_S t - T_X$$

$$(J_X + I_X/2)\ddot{\theta}_Y + (D + D_R)\dot{\theta}_Y + \{K - (I_X - I_Z/2)\omega_S^2\}\theta_Y - (J_Z + I_X)\omega_S \cdot \dot{\theta}_X - (T_D + D \cdot \omega_S)\theta_X = q_Y \cos 2\omega_S t - q_X \cdot \sin 2\omega_S t - T_Y \quad (4)$$

where $q_X$ and $q_Y$ are given by

$$q_X = (I_X/2)\ddot{\theta}_X + I_X \cdot \omega_S \cdot \dot{\theta}_Y - (I_X - I_Z/2) \cdot \omega_S^2 \cdot \theta_X$$

$$q_Y = (I_X/2)\ddot{\theta}_Y - I_X \cdot \omega_S \cdot \dot{\theta}_X - (I_X - I_Z/2) \cdot \omega_S^2 \cdot \theta_Y$$

The coefficient $(T_D + D \cdot \omega_S)$ is known as the cross-axis torque constant. Terms associated with this coefficient, as well as the damping coefficient $(D + D_R)$, can be dropped out from relations (4) as a first approximation since their contributions are negligible compared to the rest of the terms. The effective restraint torque coefficient given by

$$[K - (I_X - I_Z/2) \cdot \omega_S^2]$$

that appears in Eqs. (4) is of considerable importance. If it is set to zero, the response will have the characteristics of a free gyro, i.e., a gyro with no elastic restraint torques. This is achieved by spinning the rotor at $\omega_S$ given by

$$\omega_S = \sqrt{(K_X + K_Y)/(I_X + I_Y - I_Z)} \quad (5)$$

which is known as the *tuning condition*. A flexure-mounted gyro that satisfies Eq. (5) is known as a DTG. By dropping the insignificant terms and implementing the tuning condition in relations (4), the following simplified model for the DTG is obtained

$$J_* \cdot \ddot{\theta}_X + H_* \cdot \dot{\theta}_Y = -q_X \cdot \cos 2\omega_S \cdot t - q_Y \cdot \sin 2\omega_S \cdot t - T_X$$

$$J_* \cdot \ddot{\theta}_Y - H_* \cdot \dot{\theta}_X = q_Y \cdot \cos 2\omega_S \cdot t - q_X \cdot \sin 2\omega_S \cdot t - T_Y \quad (6)$$

where

$$J_* = J_X + I_X/2; \qquad H_* = (J_Z + I_X)\omega_S$$

These are the equations of a coupled oscillator that is subjected to an input disturbance at exactly double the shaft spin. An almost complete elimination of the $q_X$ and $q_Y$ terms is theoretically feasible using a multigimballed rotor.

## Hinge

The hinge, quite often called the flexible joint, is the most critical part of the DTG and its design and manufacture call for the most sophisticated technologies in the aerospace industry. There are as many variations of the hinge design as there are manufacturers of DTGs around the world. A large number of hinge patents are available. Bilinski et al.,[18] Ensinger et al.,[19-21] Krupick et al.,[22] Craig,[23] and Wyse[24] are but a few examples. Scieszko and Mansour[25,26] reported on some design aspects of a class of flexible joints.

Figure 4 shows the schematics of a hinge that makes use of torsion bars carved by electroerosion. This type of hinge contains three or four parts that have to be carefully aligned, cemented (or welded), and then treated for stress relief. Figure 5 illustrates the schematics of another design of a hinge that is built from 51 separate pieces. Since many of these pieces are identical, the final assembly will contain only six different parts. The blades are photoetched from a precision-rolled strip whose thickness is controlled to $\pm 1.5\ \mu$. Fabrication is achieved by chemically depositing a very thin layer of a special alloy material onto certain components prior to assembly. By raising the temperature under vacuum, the alloy melts and is pulled into the joint by capillary action.

Figure 6 gives the schematics of another hinge built from only two parts. Two cylinders are machined to fit one inside the other with tight tolerance. Next, the cylinders are secured together coaxially, while half the flexure blades are carved along two mutually perpendicular axes as shown in Fig. 6a. An electroerosion machine of the wire-cutting type is used to perform this cutting. Finally, one cylinder is rotated 90 deg relative to the other, then fixed permanently by cement or laser-welding. The remaining carving is performed on the two cemented cylinders as shown in Fig. 6b.

Monobloc hinges, illustrated in Fig. 7, are used by a number of manufacturers. DIGICON S.A. in Brazil has designed and developed the necessary technology for the fabrication and testing of a variation of the monobloc hinge.

The hinges described in Figs. 4–7 are examples of configurations used by Litton, Singer, Teledyne, Condor Pacific, and Incosym in the United States; Sagem and Sfim in France; British Aerospace and Smith Industries in the United Kingdom; Litef in Germany; and Litton Italia in Italy. More details about these suppliers can be found in Brown.[7]

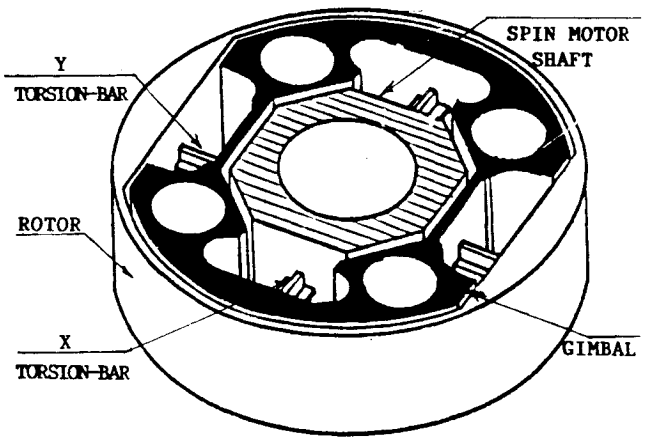


Fig. 4 Hinge with torsion bars.

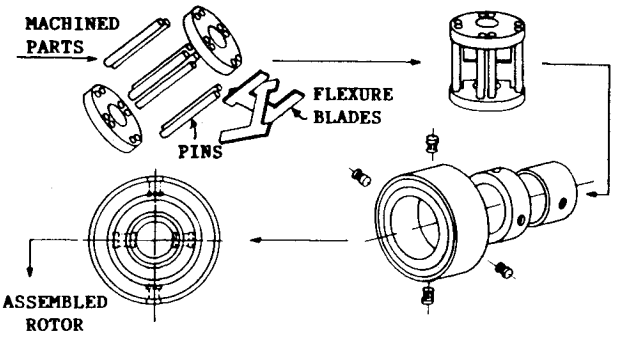


Fig. 5 Hinge with 51 pieces.

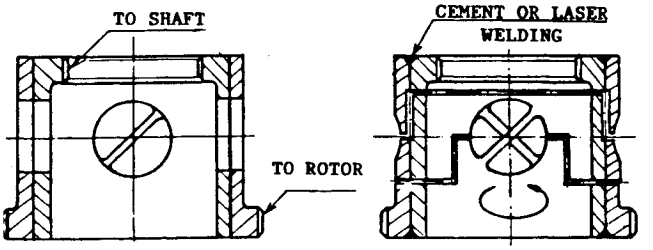


Fig. 6 Two-part hinge.

All types of hinges have to satisfy the following requirements.

### Alignment

The geometric axes of the hinge should be mutually orthogonal to each other within a given tolerance and all should pass through an imaginary sphere of a given radius. When mounted to the shaft, the rotor should have its center of mass coinciding with the geometric center of flexure of the hinge within predetermined limits. The rotor should be provided with means for coarse alignment of the two centers. A shaker is used for fine alignment, together with axial screws as additional weights.

### Tuning

The tuning condition should be satisfied. The $K$s, the $I$s, and the value of $\omega_S$ should be selected to satisfy relation (5). Fine tuning is achieved mechanically by adjusting the $I$s of the gimbal by using the screws. Tuning can also be achieved by adjusting the spin speed $\omega_S$ electronically to satisfy relation (5).

### Acceleration Capabilities

The flexure members have to be checked for mechanical integrity. The flexures can fail at the root sections because of buckling and/or shear stress due to excessive axial and/or lateral accelerations imparted to the gyro rotor. A closed-form solution or finite-element approach is normally used in the early phases of design to evaluate the capabilities of the hinge for lateral and axial accelerations.

### Leaf Angle

Research conducted at DIGICON S.A. showed that for a monobloc hinge, the angle of the leaf with respect to the axis of spin, among other parameters, plays an important role in the anisoelastic drift of the DTG. In fact, this type of drift can be almost eliminated by the proper choice of the leaf angle.

### Dimensional Stability

The alloy selected for the hinge and the process of fixation of the hinge to the rotor and the spin shaft should guarantee the dimensional stability of the assembly under severe conditions of operation ($-40$ to $+75$°C). Each rotor-hinge subassembly normally undergoes thermal treatment for several weeks in programmable ovens with monitored thermal cycles.

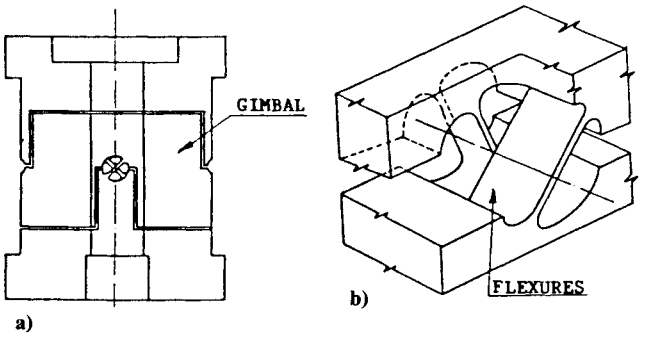


Fig. 7 Monoblock hinge.

## Torquer

The torquer is that part of the DTG responsible for imparting the proper moments to the rotor to maintain its axis of rotation aligned with the spin axis, i.e., to maintain a zero gap difference at all times. Torquing is achieved by using the interaction between a coil-carrying current and a magnetic field of fixed strength. There are several ways to achieve the torquing effect. Figure 8 shows the elements of a typical torquer.

### Permanent Magnets

The radial magnetic field is created by permanent magnets of a rare-earth element and cobalt. They are selected to give the maximum possible flux density, highest magnetomotive force per unit volume, and most stable magnetic characteristics for a wide range of temperature variations. The radial field can be created by using segmented rings that are radially magnetized. Axially magnetized cylinders assisted by pole rings can also be used to create the radial field.

The permanent magnets are normally secured to the rotor by special cements that are carefully cured and thermally soaked to ensure dimensional stability. The permanent magnet is the most expensive single component that enters into the manufacture of the DTG. One segmented ring magnet can cost more than 20 times the price of one high-precision ball bearing in the DTG.

### Torquer Coils

The four coils are equally spaced in the radial magnetic field. They function in diametrically opposite pairs. The $\ell_c$ is chosen to maximize $F$, which results from the interaction of $B_a$ with $i_t$ in the torquer coils. The distance between adjacent coils should be such that electronic noise and cross-talk are minimum. Coils are placed to intercept equal and opposite radial magnetic fields on the curved lengths of each coil. The straight part of the coil is chosen as short as possible to minimize heat losses. Double-enamel wire is used for the coils.

### Pickoffs

Pickoffs are sensors to detect variations in the gaps between the rotor and the gyro case as shown in Fig. 8. There are many types of pickoffs in use. The most common type is electromagnetic variable reluctance with an excitation frequency of several kHz to minimize noise contamination. The four pickoffs are equally spaced and fixed to the gyro case. The diametrically opposite pairs have to be impedance matched.

### Operation

The output signals from the $X$ and $Y$ pickoffs are zero in the absence of angular rotations. If an angular velocity $\omega_Y$ is imparted to the case about its $Y$ axis, as shown in Fig. 8, the following sequence occurs:

1) Gap $g_{X1}$ will be different from $g_{X2}$. The $X$ pickoffs will be active, whereas the $Y$ pickoffs will remain idle.

2) To cancel the difference between the gaps, the torquer should impart a torque about the case-fixed $X$ axis that will force the rotor to precess about the $Y$ axis with an angular velocity $\omega_D$.

3) The signal from the $X$ pickoffs is used to inject a current $i_t$ in the $Y$ torquer coils. This current creates a system of forces $F$ on the curved length of the $Y$ coils and, in turn, this gives rise to the required reaction torque $T_X$.

4) The current $i_t$ will only vanish when the difference between the gaps becomes zero. The highest attainable value of $\omega_D$ is the dynamic range of the DTG.

### Temperature Sensitivity

In the design and use of DTGs, one should notice that

1) With the increase of temperature, the $B$-$H$ demagnetization curves dislocate to the right and the optimum load line rotates as shown in Fig. 9. The tendency is that $B_a$ decreases as the temperature increases. A larger $i_t$ is used to produce the same torque.

2) The $\rho_e$ and consequently $R$ increase with the temperature. This implies that the $i_t^2 R$ losses will further increase with temperature.

3) The $h$ is a temperature-dependent parameter and its value will dictate the level of the steady-state temperature of the coil.

### Design Strategy of the Torquer

The basic equations, in vector form, are given by

$$T_X = \omega_D \times H; \qquad F = n\ell_c i_t \times B_a$$

from which one obtains the following scalar relation:

$$(n \cdot i_t) = (\omega_D \cdot H)/(2B_a \cdot \ell_c \cdot d_c) \tag{7}$$

A preliminary definition of the torquer is possible if we assume that the following quantities are already selected: $\{\omega_D, H, d_c, E, P_m, h, \rho_e\}$ and the magnetization curves. All of the coefficients that are not dependent on the temperature can be evaluated in advance.

The iterative steps for the preliminary design are as follows:

1) A value $\theta$, the temperature of the coil, is assumed.

2) By using the current value of $\theta$, the values of $h$ and $\rho_e$ and the equation of the optimum load line are obtained.

3) The $B$ is evaluated using the proper demagnetization curve.

4) $(n \cdot i_t)$ is evaluated using relation (7).

5) The $d_b$ is evaluated using

$$d_b = \sqrt{4\rho_e P_m (n \cdot i_t)/(\pi E)} \tag{8}$$

6) The $n$, $i_t$, and $R$ are easily evaluated in that order.

7) By using $i_t^2 \cdot R$ and $h$, the steady-state temperature $\theta_s$ is evaluated.

8) If $\theta_s$ is close to $\theta$, the iterations are terminated; otherwise, $\theta$ is replaced by $\theta_s$ and one starts again with step 2. A finite-element analysis is recommended to evaluate the effects of fringing and leakage in the magnetic circuit.

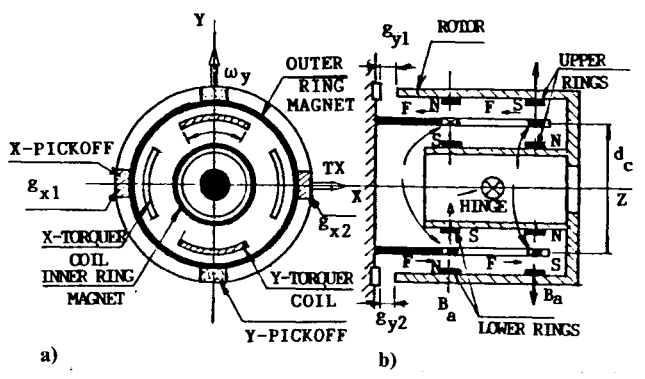


Fig. 8 Gyro's torquer.

## Gyroscopic Drifts

The error in the output signal of a gyro is referred to as its gyroscopic drift and is normally reported in deg/h. It is important to evaluate these drifts accurately for the proper use of a DTG. There are two basic types of drifts.

### Compensable Drifts

Compensable drifts are errors that can be modeled. They are repeatable and/or measurable in a laboratory environment to a high degree of accuracy. These drifts can be minimized through the proper design of the different components or compensated in full or in part by using hard and/or software. To this class belong the following:

1) Non-$g$-sensitive drifts whose values are independent of the velocities or accelerations applied to the gyro. They appear due to the structural damping in the hinge, mistuning of the spin shaft speed, electronic bias in the pickoffs, the mismatch of the flexure stiffness and eddy magnetic fields. This type of drift is often called *bias*.

2) Direct and quadrature components of $g$-sensitive drifts whose values depend on the magnitude of the lateral accelerations applied to the rotor. They appear due to the mismatch of the center of mass of the rotor and the geometric center of the flexure.

3) Drifts that are due to the misalignments of the gyro case axes with respect to the nominal gyro axes.

4) Anisoelastic drifts whose values depend on the simultaneous presence of an axial and a lateral acceleration. Careful design can minimize this type of drift.

### Uncompensable Drifts

Uncompensable drifts are random in nature and principally caused by inevitable changes in the positions of the spheres of the roller bearings during operation, transient temperature fields that affect the aerodynamic forces on the rotor, and thermal changes that modify the performance of the critically dimensioned magnetic circuits. These drifts are described by two quantities: 1) day-to-day drift, quite often referred to as repeatability (each time the gyro is switched off and then on again under the same input conditions, a different output from the gyro is obtained) and 2) random drift (for prolonged periods of operation under the same input conditions, the output of the gyro will undergo some changes). These drifts cannot be easily compensated because they are only predictable on a probabilistic basis. The quality of a DTG is normally assessed by the values of is dynamic range, its day-to-day drift, and its long-term drift.

## Mass Unbalance Drift

Mass unbalance drift is a typical example of the appearance of a bias, as well as a harmonic disturbance at twice the spin frequency due to the axial mismatch of the center of mass of the rotor and the geometric center of flexure of a DTG as shown in Fig. 10. The $W_r$ is assumed to act in the vertical plane (0). Axes 1 and 2 are taken along the flexure bars. The angle between the two axes is $(\psi + \pi/2)$, where $\psi$ is an error angle.

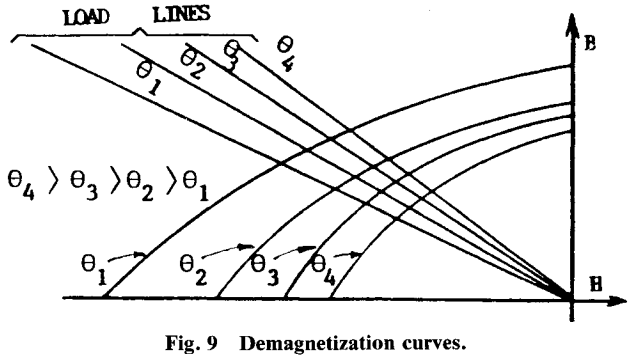


Fig. 9 Demagnetization curves.

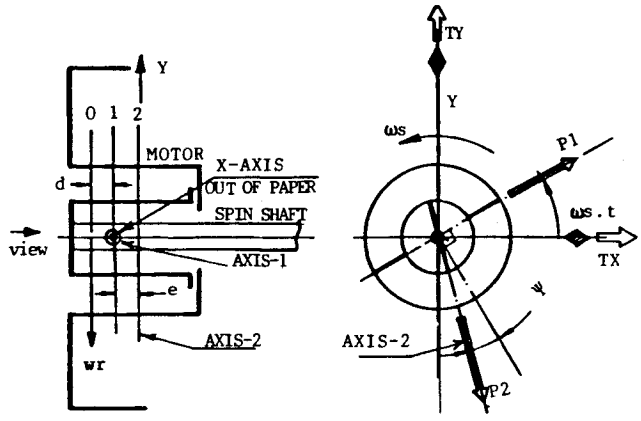


Fig. 10 Mass unbalance drift.

Planes (0), (1), and (2) are parallel to each other, with plane (1) containing axis 1 and plane (2) containing axis 2. The rotor is assumed to have an angular velocity of spin $\omega_S$. It is possible to show that $W_r$ will induce a moment that has components $P_1$ and $P_2$ along the flexures given by

$$P_1 = \left[W_r \cdot d \cdot \cos(\omega_S \cdot t - \psi)\right]/\cos\psi$$

$$P_2 = W_r\left[e \cdot \sin(\omega_S \cdot t - \psi) + (d \cdot \sin\omega_S \cdot t)/\cos\psi\right]$$

$P_1$ and $P_2$ can be decomposed along the $X$ and $Y$ case-fixed axes to obtain

$$T_X = W_r \cdot (d + e/2) + W_r \cdot e \times \left[(\cos 2\psi)\cdot\cos 2\omega_S \cdot t + (\sin 2\psi)\cdot\sin 2\omega_S \cdot t\right]/2$$

$$T_Y = W_r \cdot e \cdot \left[(\sin 2\psi)\cdot\cos 2\omega_S \cdot t - (\cos 2\psi)\cdot\sin 2\omega_S \cdot t\right]/2$$

$T_X$ and $T_Y$ are moments that have to be opposed by the torquer to maintain zero gap difference. The gyro will thus indicate the presence of angular rotations that do not exist about the $X$ and $Y$ axes. That is drift. In fact, only the dc components of $T_X$ and $T_Y$ are responsible about the drift. Thus, one obtains

$$\delta_{Xg} = 0; \quad \delta_{Yg} = (W_r/H)\cdot(d + e/2)\cdot(180/\pi) \times 3600 \qquad (9)$$

## Anisoelastic Drift

The case of the simultaneous presence of $a_Z$ and $a_X$ will be examined here. Inertia forces on the rotor are decomposed along axes 1, 2 and the spin axis. They are denoted by $F_1$, $F_2$, and $F_3$, respectively. The inertia forces on the gimbal are denoted by $f_1$, $f_2$, and $f_3$. These inertia forces and their associated deflections are shown in Fig. 11 and are given by

$$F_1 = (W_r \cdot a_X \cdot \cos\omega_S \cdot t)/g; \qquad F_2 = (W_r \cdot a_X \cdot \sin\omega_S \cdot t)/g$$

$$F_3 = W_r \cdot a_Z/g; \qquad f_1 = (1+\rho)\cdot F_1$$

$$f_2 = (1+\rho)\cdot F_2; \qquad f_3 = (1+\rho)\cdot F_3 \qquad (10a)$$

Since the flexures are identical, one can write

$$K_1 = k_2; \qquad K_2 = k_1; \qquad K_3 = k_3 \qquad (10b)$$

An inertia force $F_j$ on the rotor will induce a deflection $\Delta_j$ and an inertia force $f_j$ on the gimbal will induce a deflection $\delta_j$. These deflections are given by

$$\Delta_j = F_j/K_j; \qquad \delta_j = f_j/k_j \qquad (j = 1,2,3) \qquad (10c)$$

A careful examination of the forces and deflections shown

in Fig. 11 yields the following relations for the anisoelastic torques $T_1$, $T_2$, $T_3$, and $T_4$ about the flexures:

$$T_1 = F_2 \cdot \Delta_3 + f_2 \cdot \delta_3; \qquad T_2 = F_3 \cdot \Delta_2 + f_3 \cdot \delta_2$$

$$T_3 = F_1 \cdot \Delta_3 + f_1 \cdot \delta_3; \qquad T_4 = F_3 \cdot \Delta_1 + f_3 \cdot \delta_1 \qquad (10d)$$

These can be decomposed along the $X$ and $Y$ case-fixed axes

$$T_X = (T_2 - T_1) \cdot \sin \omega_S \cdot t - (T_3 - T_4) \cdot \cos \omega_S \cdot t$$

$$T_Y = (T_2 - T_1) \cdot \cos \omega_S \cdot t + (T_3 - T_4) \cdot \sin \omega_S \cdot t \qquad (10e)$$

Combining relations (10a) to (10e) inclusive, one obtains

$$T_X = (W_r/g)^2 \cdot a_X \cdot a_Z \cdot \left[ (2+2\rho+\rho^2)\left(\frac{1}{K_1} + \frac{1}{K_2} - \frac{2}{K_3}\right) + \rho(2+\rho)\left(\frac{1}{K_1} - \frac{1}{K_2}\right) \cos 2\omega_S \cdot t \right] \Big/ 2$$

$$T_Y = (W_r/g)^2 \cdot a_X \cdot a_Z \cdot \left[ \rho(2+\rho)\left(\frac{1}{K_1} - \frac{1}{K_2}\right) \cdot \cos 2\omega_S \cdot t \right] \Big/ 2$$

which shows that the anisoelastic drifts are given by

$$\delta_{Xgg} = 0$$

$$\delta_{Ygg} = (W_r^2/2H)(2+2\rho+\rho^2)\left(\frac{1}{K_1} + \frac{1}{K_2} - \frac{2}{K_3}\right)(180/\pi) \times 3600 \qquad (11)$$

It is noted that through careful design this drift can be eliminated by satisfying the following condition:

$$\frac{1}{K_1} + \frac{1}{K_2} - \frac{2}{K_3} = 0 \qquad (12)$$

## Error Model

The development of an accurate analytical error model is quite lengthy and complex. The model varies in form, depending on the degree of sophistication and requirements of the application.

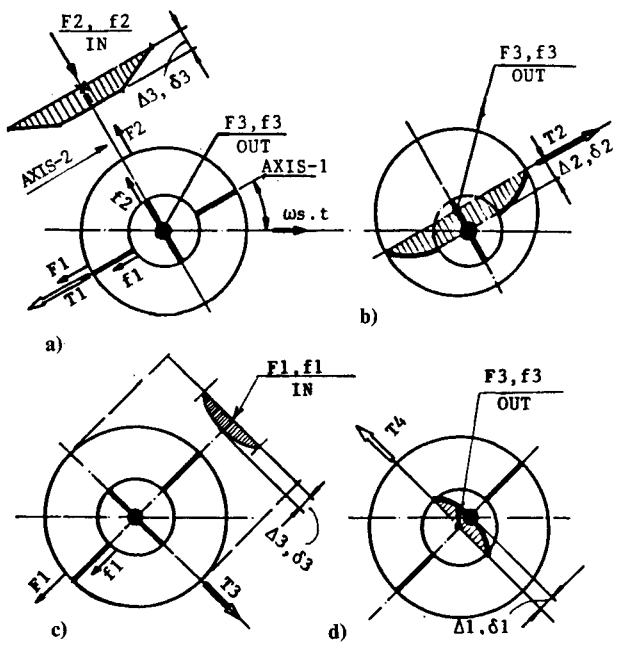


**Fig. 11 Anisoelastic drifts: a) $T_1 = \Delta_3 \cdot F_2 + \delta_3 \cdot f_2$; b) $T_2 = \Delta_2 \cdot F_3 + \delta_2 \cdot f_3$; c) $T_3 = \Delta_3 \cdot F_1 + \delta_3 \cdot f_1$; and d) $T_4 = \Delta_1 \cdot F_3 + \delta_1 \cdot f_3$.**

### Linear Model

The dynamics of the gyro are described by relations (1–3). The following simplifying assumptions are adopted:

1) $q_X$ and $q_Y$ coefficients are suppressed.
2) The tuning condition is satisfied.
3) Gimbal inertias are negligible compared to the rotor's.
4) The first derivative of $\{\phi\}$ exists; thus, the elements of the $L$ matrix will contribute to the model. One obtains

$$T_X = -(J_X\ddot{\theta}_X + H\dot{\theta}_Y + H\omega_Y) - \epsilon_X$$

$$T_Y = -(J_X\ddot{\theta}_Y - H\dot{\theta}_X - H\omega_X) - \epsilon_Y \qquad (13)$$

where $\epsilon_X$ and $\epsilon_Y$ are the error torques to a first degree of approximation. They are given by

$$\epsilon_X = J_X \cdot \dot{\omega}_X + (D + D_R) \cdot \dot{\theta}_X + (T_D + D \cdot \omega_S) \cdot \theta_Y$$

$$\epsilon_Y = J_X \cdot \dot{\omega}_Y + (D + D_R) \cdot \dot{\theta}_Y - (T_D + D \cdot \omega_S) \cdot \theta_X \qquad (14)$$

### Nonlinear Model

One starts with the following basic vectorial relation:

$$\boldsymbol{T}_c = \left(\frac{\mathrm{d}}{\mathrm{d}t}\right)_c \boldsymbol{H}_c + \boldsymbol{\omega}_c \times \boldsymbol{H}_c$$

where the subscript $c$ indicates that the vectors and differentiation are all referred to the gyro case axes. The necessary lengthy transformations and operations can be performed by assuming small rotor deflections. One can drop second-order products. Adopting the same simplifying assumptions mentioned before, Bortz[27] obtained an expression for the error model that contains all of the terms given by relations (14), plus additional terms for $\epsilon_X$ and $\epsilon_Y$ denoted by $\epsilon_{*X}$ and $\epsilon_{*Y}$, respectively. They are given by

$$(\epsilon_{*X}) = -(J_Z - J_X)(\omega_Y \cdot \omega_Z) - \theta_X \cdot \left[H \cdot \omega_Z - (J_Z - J_X) \times (\omega_Z^2 - \omega_Y^2)\right] - \theta_Y \cdot \left[(J_Z - J_X)(\omega_Y \cdot \omega_X + \dot{\omega}_Z)\right]$$

$$(\epsilon_{*Y}) = (J_Z - J_X)(\omega_X \cdot \omega_Z) + \theta_Y \cdot \left[H \cdot \omega_Z + (J_Z - J_X) \times (\omega_Z^2 - \omega_X^2)\right] - \theta_X \cdot \left[(J_Z - J_X)(\omega_X \cdot \omega_Y + \dot{\omega}_Z)\right]$$

which represent a more realistic error model.

### Practical Error Models

It should be realized by now that the gyroscopic drifts due to mass unbalance and anisoelasticity, which were discussed separately before, represent additional terms in the error vector $\epsilon$. Different sophisticated error models have been reported on by Craig,[28] Handrich,[29] and Britting.[30] Those models took into account some of the following sources of errors:

1) Errors due to the mismatch of torsional flexures.
2) Errors due to the misalignment of gyro case axes with the nominal axes.
3) Errors due to mistuning.
4) Errors that occur at a frequency equal to the spin frequency. They are called the 1 N errors. To this class belong the motor dynamics.
5) Errors that occur at a frequency equal to twice the spin frequency. They are called the 2 N errors.
6) The scale factors are represented by

$$S_X = S_{X0} \cdot (1 + \epsilon_{SX}); \qquad S_Y = S_{Y0} \cdot (1 + \epsilon_{SY})$$

where $S_{X0}$ and $S_{Y0}$ are the nominal values of the scale factors. The scale factor errors $\epsilon_{SX}$ and $\epsilon_{SY}$ are normally expressed in power series expansions

$$\epsilon_{SX} = \sum_{i=0}^{\infty} cx_i \cdot \omega_X^i; \qquad \epsilon_{SY} = \sum_{i=0}^{\infty} cy_i \cdot \omega_Y^i \qquad (15)$$

## Gyro Testing

A DTG is subjected to a number of tests during its evolution and use. These are as follows:

1) Development tests that are intended to help introduce necessary changes in the design in time.

2) Qualification tests that are performed on the prototype to verify that the DTG meets the basic requirements in service: endurance to shocks, vibrations, temperature variations, etc.

3) Acceptance tests that are conducted on each DTG after its manufacture and assembly. They are normally made at the supplier's site in the presence of the user's representatives. These tests are conducted to ensure that the performance of the DTG is within the required specifications.

4) Calibration tests that are performed on the DTG, together with its electronics. They are conducted at the user's site to ensure its proper functioning at the system's level.

Only the acceptance tests will be briefly discussed here since they form an important part of gyro manufacture. In these tests, one is able to measure $\tau_r$, $(S_X,S_Y)$, $(B_X,B_Y)$, $m$, $q$, $(r_X,r_Y)$, $(d_X,d_Y)$, and $(R_X,R_Y)$. The procedures and protocols for conducting the acceptance tests vary from one manufacturer to another. In this paper, we shall report the simplest.

### Test Cube

Figure 12 shows a granite cube used to house the DTG during the acceptance tests. The orthogonalities and parallelism among the outer and inner surfaces of the cube are held within tight tolerances. The inner case is made of a special alloy of high dimensional stability. The test cube is provided with references (dowels) to guarantee that, when the DTG is placed inside it, the DTG will have its $X$ and $Y$ case-fixed axes perpendicular to the outside surfaces of the cube. The cube containing the DTG is placed on a granite table that is rigidly fixed to a heavy seismic mass. The surface of the table is machined within microns and leveled to the local horizontal. A granite bar of rectangular cross section is machined to tight tolerances and fixed (cemented) to the granite table in an east-west direction. When the cube is brought into contact with the bar, the normal line to the contacting surfaces of the cube and the bar should point to the true geographic north within arc minutes.

### Four-Position SAV Test

The test cube is held against the granite bar in four different positions maintaining, for each one of them, the positive spin axis vertically upward. An examination of Fig. 13 yields the following relations:

$$S_X \cdot X_1 = B_X; \qquad S_Y \cdot Y_1 = B_Y + \Lambda \cos \lambda$$

$$S_X \cdot X_2 = B_X + \Lambda \cos \lambda$$

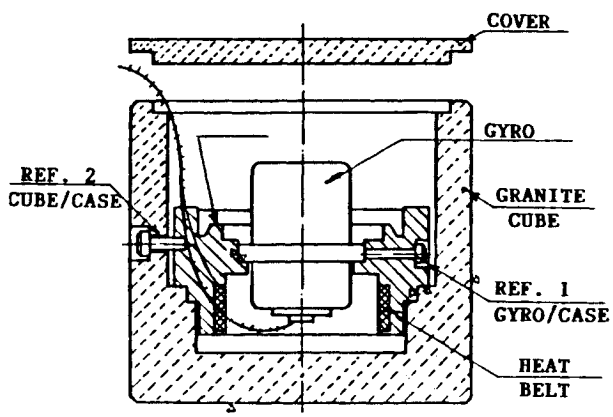


Fig. 12 Test cube.

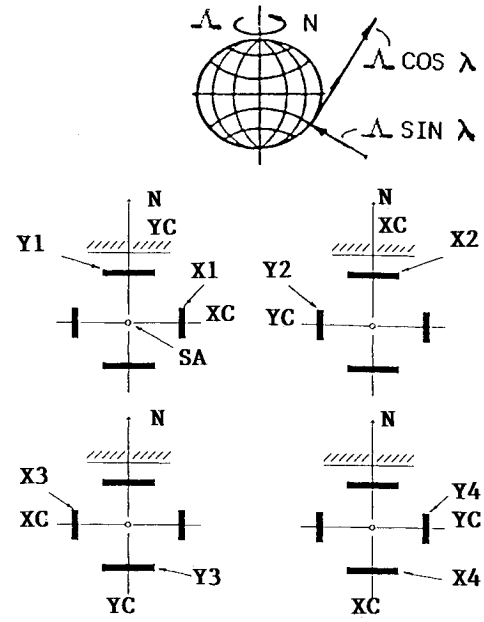


Fig. 13 Four-position *SAV* test.

$$S_Y \cdot Y_2 = B_Y; \qquad S_X \cdot X_3 = B_X; \qquad S_Y \cdot Y_3 = B_Y - \Lambda \cos \lambda$$

$$S_Y \cdot Y_4 = B_Y; \qquad S_X \cdot X_4 = B_X - \Lambda \cos \lambda$$

The $(X_j,Y_j)$ for $j=1,2,3$, and 4 are the $X$ and $Y$ torquer currents in the four positions. Combining the previous relations, one obtains

$$S_X = (2\Lambda \cos \lambda)/(X_2 - X_4); \qquad S_Y = (2\Lambda \cos \lambda)/(Y_1 - Y_3)$$

$$B_X = S_X \cdot (X_1 + X_2 + X_3 + X_4)/4$$

$$B_Y = S_Y \cdot (Y_1 + Y_2 + Y_3 + Y_4)/4 \tag{16}$$

### Four-Position SAH Test

The four positions are executed with the positive spin axis in a horizontal plane and pointing north as shown in Fig. 14. Recalling the discussion given before about the mass unbalance, one can write

$$S_X \cdot X_1 = B_X - q; \qquad S_Y \cdot Y_1 = B_Y + m - \Lambda \sin \lambda$$

$$S_Y \cdot Y_2 = B_Y + q; \qquad S_X \cdot X_2 = B_X + m - \Lambda \sin \lambda$$

$$S_X \cdot X_3 = B_X + q; \qquad S_Y \cdot Y_3 = B_Y - m + \Lambda \sin \lambda$$

$$S_Y \cdot Y_4 = B_Y - q; \qquad S_X \cdot X_4 = B_X - m + \Lambda \sin \lambda$$

The $m$ and $q$ are the drifts that will normally contaminate the output of the DTG in that configuration due to mass unbalance. Combining the previous relations, one obtains the following expressions:

$$m = \Lambda \cdot \sin \lambda + \left[S_X \cdot (X_2 - X_4) + S_Y \cdot (Y_1 - Y_3)\right]/4$$

$$q = \left[S_X \cdot (X_3 - X_1) + S_Y \cdot (Y_2 - Y_4)\right]/4 \tag{17}$$

### Random Drifts

The gyro is placed on the granite table, with its positive axis pointing vertically upward and the $Y$ torquer axis pointing north. The DTG is turned on and left until it reaches a stable operating temperature. After that, the currents in the $X$ and $Y$ torquer coils are recorded at equal intervals of time (normally every 10 min). A number $nn$ of data points is collected

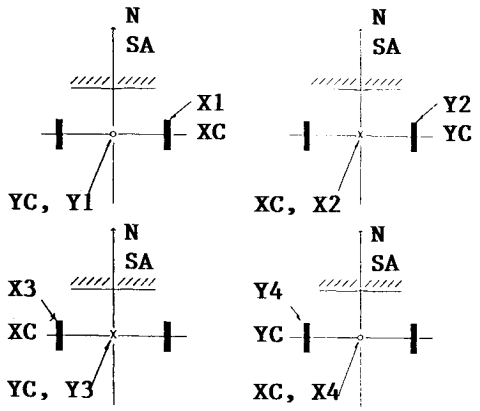


**Fig. 14 Four-position *SAH* test.**

(normally 12). The data points are denoted by $(X_j, Y_j)$ for $j = 1,2,\ldots,nn$. The $1\sigma$ values of random drifts are given by

$$r_X = S_X \cdot \sqrt{\left[\sum_{j=1}^{j=nn} (X_j^2)\right]/(nn-1)}$$

$$r_Y = S_Y \cdot \sqrt{\left[\sum_{j=1}^{j=nn} (Y_j)^2\right]/(nn-1)} \tag{18}$$

**Day-to-Day Drift**

The gyro is placed on the granite table as in the random drift tests. The DTG is turned on and left until the transients settle. Next, a series of off-on cycles are applied to the power supply of the gyro. Normally, each cycle has a period of 30 s of power off, followed by 2 min of power on. These cycles are repeated *mm* times (normally six). The currents in the torquer coils are recorded just before the power supply is switched off. The data points are denoted by $(X_j, Y_j)$ for $j = 1,2,\ldots,mm+1$. The $1\sigma$ values of repeatability are

$$d_X = S_X \cdot \sqrt{\left[\sum_{j=1}^{j=mm+1} (X_j)^2\right]/mm}$$

$$d_Y = S_Y \cdot \sqrt{\left[\sum_{j=1}^{j=mm+1} (Y_j)^2\right]/mm} \tag{19}$$

## Conclusions

A review of the recent advances in DTG technologies has been presented. The reader is referred to Mackenzie[31] for an interesting survey of gyro history. Careful attention should be given to many other design issues, such as high-precision bearings, the hysteresis motor, the inert gas used to fill a gyro, feed-thrusts, the temperature and velocity sensors inside the gyro case, and caging loops.

This paper has barely touched on a challenging field that calls upon the expertise of researchers in different disciplines: dynamics, materials, manufacturing techniques, electronics, software, simulation, optimization, testing, control systems, and instrumentation. These have to be coordinated to achieve the optimum performance of a product that is normally double the size of a matchbox.

## References

[1]Royal Aircraft Establishment, "Note on the Proposal for an Oscillogyro," I.A.P. 982-UDC 531.383, Aug. 1948.

[2]Barnes, J. W., "Oscillogyro-Ferranti," British Patent No. 599,826, Sept. 1961.

[3]Howe, E.W., "Gyroscope Apparatus," U.S. Patent No. 3,301,073, Jan. 31, 1967.

[4]Howe, E. W., "Gyroscopic Apparatus and Systems," U.S. Patent No. 3,477,298, Nov. 11, 1969.

[5]Krupick, W. J., et al., "Two-Axis Gyro," U.S. Patent No. 3,354,726, Nov. 28, 1967.

[6]Erdley, H. F., "Gyroscope Having Vibrating Gimbals," U.S. Patent No. 3,678,764, July 25, 1972.

[7]*Inertial System Requirements,* R. G. Brown Associates, Vols. 1 and 2, 1987.

[8]Savet, P. H., "Dynamics of Ideal Suspensions Applied to Rotating Bodies in Space," AIAA 2nd Annual Meeting, July 1965 (Paper 65-435).

[9]Lipman, J. S., "Application of the Complex Method to Transform Analysis of Spinning Systems with Rotating Non-Symmetries," *Proceedings of the Joint Automatic Control Conference* (Ann Arbor, MI), IEE Congress, June 1968.

[10]Craig, R. J. G., "Theory of Operation of an Elastically Supported Tuned Gyroscope," *IEEE Transactions on Aerospace and Electronic Systems,* Vol. AES-8, No. 3, 1972, pp. 289–297.

[11]Craig, R. J. G., "Inertial Navigation Components and Systems," *AGARD Conference Proceedings,* AGARD, Neuilly Sur Seine, France, No. 116, 1972, pp. 12.1–12.17.

[12]Savage, P. G., "Strapdown Sensors," *AGARD Lecture Series 95,* June 1978, pp. 2.3–2.46.

[13]Stieler, B., and Winter, H., "Gyroscopic Instruments and Their Applications to Flight Testing," *AGARD Publication 160,* Vol. 15, 1982.

[14]"Preliminary Design of a Redundant Strapped Down Inertial Navigation Unit Using Two-Degree-of-Freedom Tuned-Gimbal Gyroscopes," NASA Document No. CR-145305, 1973.

[15]"Investigation of Application of TDF-DTD to Strapdown Navigation Systems," NASA Rept. No. CR-132419, 1974.

[16]"Two-Axis Flexure Mounted Gyroscope," Singer Document No. S/C 527, Stamford, CT, Sept. 1977.

[17]"Specification Format Guide and Test Procedure to Two-Degree-of-Freedom Dynamically Tuned Gyros," IEEE/ANSI Standard No. 813, New York, 1988.

[18]Bilinski, D. J., et al., "Universal Joint Flexure Hinge," U.S. Patent No. 3,527,062, Sept. 8, 1970.

[19]Ensinger, W. B., "Gyroscopic Flexure Hinge Suspension," U.S. Patent No. 3,585,866, June 22, 1971.

[20]Ensinger, W. B., "Gyroscopic Flexure Hinge Assembly," U.S. Patent No. 3,614,894, Oct. 26, 1971.

[21]Ensinger, W. B., et al., "Flexure Hinge Assembly," U.S. Patent No. 3,700,289 (290), Oct. 24, 1972.

[22]Krupick, W. J., et al., "Universal Joint Flexure Assembly," U.S. Patent No. 3,709,045, Jan. 9, 1973.

[23]Craig, J. G., "Gimbal Structure for Dynamically Tuned Free Rotor Gyro, U.S. Patent No. 3,832,906, Sept. 3, 1974.

[24]Wyse, S. F., "Multigimbal Flexure Universal Joint," U.S. Patent No. 3,943,778, March 16, 1976.

[25]Scieszko, J. L., and Mansour, W. M., "Analysis and Design of Leaf-Spring Flexible Joints Driving Gyroscopic Rotors," *Proceedings of 10th IMACS World Congress on System Simulation and Scientific Computation,* Concordia University, Montreal, Canada, 1982, pp. 155–157.

[26]Scieszko, J. L., and Mansour, W. M., "Analysis and Design of Composite Universal Flexure Joints," *Proceedings of ASME Congress on Computer Applications* (San Diego, CA), 1982, pp. 237–241.

[27]Bortz, J. E., "Dynamic Errors in a Tuned Flexure Mounted Strapdown Gyro," NASA Rept. No. CR-124161, 1972.

[28]Craig, R. J. G., "Theory of Errors of a Multigimbal, Elastically Supported, Tuned Gyroscopes," *IEEE Transactions on Aerospace and Electronic Systems,* Vol. AES-8, No. 3, 1972, pp. 289–297.

[29]Handrich, E., "Error Models for Strapdown Systems," *Symposium Gyro Technology* (Stuttgart, Germany), 1979, pp. 9.01–9.22.

[30]Britting, K. R., "Error Analysis of Strapdown and Local Level Inertial Systems," MIT Rept. NGR-27-009-229, NASA CR No. 107741, Nov. 1969.

[31]Mackenzie, D., *Investing Accuracy: A Historical Sociology of Nuclear Missile Guidance,* Univ. of Edinburgh, Edinburgh, Scotland, 1990.